Impulse loading resulting from shallow buried explosives in water-saturated sand

M Grujicic[1]*, **B Pandurangan**[1], **Y Huang**[1], **B A Cheeseman**[2], **W N Roy**[2], and **R R Skaggs**[2]
[1]Department of Mechanical Engineering, Clemson University, Clemson, USA
[2]Army Research Laboratory, Survivability Materials Branch, Aberdeen, Proving Ground, Maryland, USA

The manuscript was received on 2 March 2006 and was accepted for revision for publication on 13 October 2006.

DOI: 10.1243/14644207JMDA96

Abstract: A transient non-linear dynamics analysis of the detonation of a landmine buried to different depths in water-saturated sand is carried out in order to determine the resulting impulse loading. The results obtained are compared with their experimental counterparts obtained using the vertical impulse measurement fixture (VIMF), a structural mechanical device that enables direct experimental determination of the blast-loading impulse. The mechanical response of the structural steel used in the construction of the VIMF and the hydrodynamic response of the TNT high-energy high-pressure detonation products generated during detonation of a mine and of the air surrounding the VIMF are represented using the standard materials models available in the literature. The mechanical response of the sand surrounding the mine, on the other hand, is represented using the present authors' recent modified compaction model [**1**], which incorporates the effects of degree of saturation and the rate of deformation, two important effects, that are generally neglected in standard constitutive models for sand.
The results obtained indicate that the use of the modified compaction model yields a substantially better agreement with the experimentally determined impulse loads over the use the original compaction model. Furthermore, the results suggest that, in the case of fully saturated sand, the blast loading is of a bubble type rather than of a shock type, i.e. it resembles under-water explosion.

Keywords: detonation, shallow buried mine, blast loading, AUTODYN

1 INTRODUCTION

Recent experience of the US military forces in Iraq clearly showed that buried and ground-laid landmines are a major threat to the survivability of lightweight vehicles like the M1114 high mobility multi-purpose wheeled vehicles (HMMWV or Humvee) and that they present a significant challenge to fielding survivable platforms. The observed destruction arising from detonation of the landmines is the result of the large impulsive loads brought about by blast and shock waves, mine fragments, and soil ejecta. The design of survivable vehicles and platforms (targets) requires the ability to understand and quantify the impulsive detonation loads from the landmines buried in different soil media and to model the response of structures/targets of interest. Elucidation and quantification of the (time-dependent) load a buried landmine applies to a target structure above it when the landmine is detonated (typically represented by the associated total vertical impulse or by the spatial distribution of the specific impulse) is quite challenging, since such load depends on the size and shape of the charge, its depth of burial, the distance between the soil surface and the target, and the properties (density, particle size and distribution, presence of organic matter, water content, etc.) of the soil in which the landmine is buried. Direct experimental characterizations of landmine-blast events are highly critical for getting a better understanding of the accompanying enormously complex phenomena. However, it is not practical or cost-effective to carry out experimental

*Corresponding author: Department of Mechanical Engineering, Clemson University, 241, EIB, Clemson, SC 29634, USA. Email: mica@ces.clemson.edu

Report Documentation Page

Form Approved
OMB No. 0704-0188

1. REPORT DATE	2. REPORT TYPE	3. DATES COVERED
2007		**00-00-2007 to 00-00-2007**

4. TITLE AND SUBTITLE	5a. CONTRACT NUMBER
Impulse loading resulting from shallow buried explosives in water-saturated sand	5b. GRANT NUMBER
	5c. PROGRAM ELEMENT NUMBER
6. AUTHOR(S)	5d. PROJECT NUMBER
	5e. TASK NUMBER
	5f. WORK UNIT NUMBER
7. PERFORMING ORGANIZATION NAME(S) AND ADDRESS(ES) **Celmson University,Department of Mechanical Engineering,Clemson,SC,29634**	8. PERFORMING ORGANIZATION REPORT NUMBER
9. SPONSORING/MONITORING AGENCY NAME(S) AND ADDRESS(ES)	10. SPONSOR/MONITOR'S ACRONYM(S)
	11. SPONSOR/MONITOR'S REPORT NUMBER(S)

12. DISTRIBUTION/AVAILABILITY STATEMENT
Approved for public release; distribution unlimited

13. SUPPLEMENTARY NOTES

14. ABSTRACT

A transient non-linear dynamics analysis of the detonation of a landmine buried to different depths in water-saturated sand is carried out in order to determine the resulting impulse loading. The results obtained are compared with their experimental counterparts obtained using the vertical impulse measurement fixture (VIMF), a structural mechanical device that enables direct experimental determination of the blast-loading impulse. The mechanical response of the structural steel used in the construction of the VIMF and the hydrodynamic response of the TNT high-energy high-pressure detonation products generated during detonation of a mine and of the air surrounding the VIMF are represented using the standard materials models available in the literature. The mechanical response of the sand surrounding the mine, on the other hand, is represented using the present authors? recentmodified compaction model [1], which incorporates the effects of degree of saturation and the rate of deformation two important effects, that are generally neglected in standard constitutive models for sand. The results obtained indicate that the use of the modified compaction model yields a substantially better agreement with the experimentally determined impulse loads over the use the original compaction model. Furthermore, the results suggest that, in the case of fully saturated sand, the blast loading is of a bubble type rather than of a shock type, i.e. it resembles under-water explosion.

15. SUBJECT TERMS

16. SECURITY CLASSIFICATION OF:			17. LIMITATION OF ABSTRACT	18. NUMBER OF PAGES	19a. NAME OF RESPONSIBLE PERSON
a. REPORT **unclassified**	b. ABSTRACT **unclassified**	c. THIS PAGE **unclassified**	**Same as Report (SAR)**	**15**	

determination of the response of all targets of interest to buried charges of all sizes in a variety of soils. Recent advances in numerical analysis capabilities, particularly the coupling of Eulerian solvers (used to model gaseous detonation products and air) and Lagrangian solvers (used to represent vehicles/platforms an soil), have allowed simulations to provide insight into complex loading created by the mine blast event. However, a quantified understanding of the blast phenomena and loadings through computer modelling is still not mature. As discussed in the present authors' previous work [**1**], the lack of maturity of computer simulations of the blast event is mainly due to inability of the currently available materials models to realistically represent the response of the materials involved under high-deformation, high deformation-rate high-temperature conditions, and the type of conditions accompanying landmine detonation. In particular, the soil response and its dependence on the soil composition, microstructure, and water content are poorly understood [**2**].

A review of the literature shows that there exists an extensive body of work dealing with the investigation of buried charges. However, much of this work does not focus on the characterization of the blast output of landmines, but rather on cratering effects in soils, with applications towards the efficient utilization of explosives for excavation (i.e. canals, trenches, etc.) or in the survivability of structures subjected to near surface blasts [**3**].

Among the works published in the open literature, which directly deal with experimental characterization of the effects of anti-tank (AT) and anti-personnel (AP) landmine blasts, the following appear to be the most relevant to the present subject matter. Westine *et al.* [**4**] carried out experiments on a plate, which was mounted above a buried charge representing an AT landmine. The plate contained a number of through-the-thickness holes at incremental distances from the mine, in which plugs of known mass were placed. The blast accompanying mine detonation caused the plugs to be driven out of the holes and from their velocity the impulsive loading on the plate was calculated. Morris [**5**] used the results of Westine *et al.* [**4**] to construct a design-for-survivability computer code for lightweight vehicles. More recently, Bergeron *et al.* [**6**] carried out a comprehensive investigation of the buried landmine blasts using an instrumented ballistic pendulum. From these experiments, the pressure and impulse as a function of time were recorded at several locations in air directly above the mine as well as in the sand surrounding the mine, along with x-radiographs and high speed photographs of the associated soil cratering and ejecting phenomena. The work of Bergeron *et al.* [**6**] was subsequently extended by Braid [**7**] to incorporate different charge sizes, soil types, and improved instrumentation.

In the present authors' recent computational work [**8**] based on the use of AUTODYN, a general purpose transient non-linear dynamics explicit simulation software [**9**], a detailed comparison was made between the experimental results of Bergeron *et al.* [**10**] and their computational counterparts for a number of detonation-related phenomena such as the temporal evolutions of the shape and size of the over-burden sand bubbles and of the detonation-products gas clouds, the temporal evolutions of the side-on pressures in the sand and in air, etc. It was found that the most critical factor hampering a better agreement between the experiment and computational analysis is an inadequacy of the current material models for sand to capture the dynamic response of this material under blast loading conditions. Hence, the main objective of the present authors' subsequent work [**1**] was to improve the compaction materials model for sand in order to include the effects of the degree of saturation and the rate of deformation, the two important effects that were neglected in the available constitutive models for sand. The new material constitutive model for sand was subsequently validated for the case of sand with a low level of water saturation by comparing the experimental results associated with detonation of the shallow-buried and ground-laid C4 mines obtained through the use of an instrumented horizontal mine-impulse pendulum with their computational counterparts obtained via detailed numerical modelling of the same physical problem using AUTODYN.

The objective of the present work is to test the ability of the present authors' newly developed materials constitutive model for sand when used within a transient non-linear dynamics computational analysis to predict the effect of detonation associated with mines buried in fully water-saturated sand. This was done by comparing the model predictions with their experimental counterparts obtained in the work of Taylor *et al.* [**11**], who carried out large-scale experiments using the vertical impulse measurement fixture (VIMF) at the Army Research Laboratory, Aberdeen, MD. The VIMF is a unique facility that has been designed specifically to measure accurately the vertical impulse from buried charges weighing up to 8 kg.

The organization of the paper is as follows. A brief overview of the design, construction, and performance of the VIMF is given in section 2.1. The non-linear dynamics approach, the relevant materials models, and the definition of the computational problem investigated are respectively discussed in sections 2.2–2.4. The results obtained in the present work are presented and discussed in section 3. The

main conclusions resulting from the present work are summarized in section 4.

2 COMPUTATIONAL PROCEDURE

2.1 An overview of the vertical impulse measurement fixture

The VIMF is a structural mechanical device that enables direct experimental determination of the imparted blast-loading impulse via measurements of the vertical displacement of a known fixed-mass vertical guide rail that is capped with a witness plate, which serves as a momentum trap to capture the blast loading of the buried charge. The design and operation of the VIMF has been described in detail by Gniazdowski [**12**], Skaggs *et al.* [**13**], and Taylor *et al.* [**11**] and will be only briefly discussed here. A schematic drawing of the VIMF including the vertical guide rail and the orientation of the charge in the water-saturated sand is shown in Fig. 1. To create the required water-saturated sand condition, a cylindrical pit 3.65 m in diameter and 1.32 m deep is first constructed in the soil within the VIMF test area. To retain water in the sand pit and to keep the sand–water mixture separate from the rest of the sand, the walls of the pit are lined with 0.32 cm thick poly ethylene sheets and the pit floor is built using a commercial swimming pool liner. Once the pit liners are in place, a series of water hoses is placed in pit bottom to allow the introduction of water into the pit from the bottom. Next, approximately 14.2 m^3 of commercially available (Quickrete) sand is placed in the pit. The sand typically consists of 94.4 per cent sand, 0.3 per cent gravel, and 5.3 per cent silt/clay. The maximum dry-sand density is 1.49 g/cm^3, whereas the maximum wet-sand density is 1.91 g/cm^3. Prior to each test, water is allowed to fill the sand pit until standing water is observed on top of the sand.

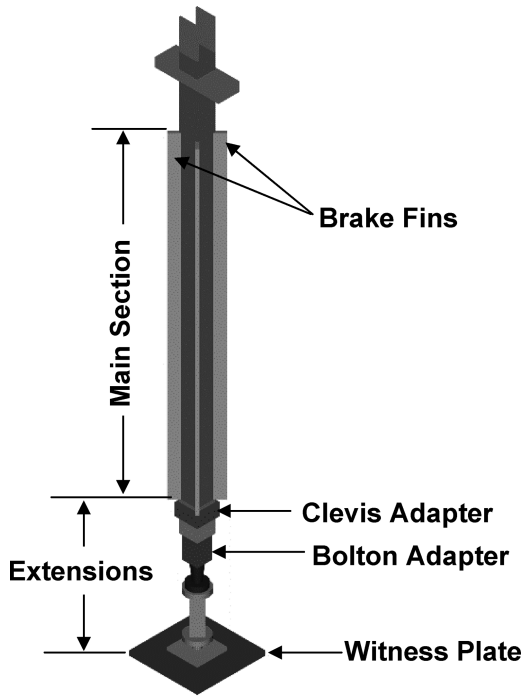

Fig. 1 The vertical impulse measurement fixture

2.2 Non-linear dynamics modelling of detonation phenomena

All the calculations carried out in the present work were done using AUTODYN, a general purpose non-linear dynamics modelling and simulation software [**9**]. In this section, a brief overview is given of the basic features of AUTODYN, emphasizing the aspects of this computer program that pertain to the problem at hand and that were not discussed in the present authors' previous work [**1**, **8**].

A transient non-linear dynamics problem is analysed within AUTODYN by solving simultaneously the governing partial differential equations for the conservation of momentum, mass, and energy along with the materials constitutive equations and the equations defining the initial and the boundary conditions. The equations mentioned above are solved numerically using an explicit scheme and one of the two basic mathematical approaches, the Lagrange approach and the Euler approach. Within AUTODYN these approaches are referred to as processors. The key difference between the two basic processors is that within the Lagrange processor, the numerical grid is attached to and moves along with the material during calculation, whereas within the Euler processor, the numerical grid is fixed in space and the material moves through it. The exact mathematical formulations of the governing differential equations are different within the two processors and their details will not be presented in the current work, but can be found in reference [**9**]. Nevertheless, in order to show how the governing differential equations and the materials constitutive models define a self-consistent system of equations for the dependent variables (nodal displacements, nodal velocities, cell material densities, and cell internal energy densities), a brief description is given below for the case of the Lagrange processor.

The momentum conservation equation relates the nodal accelerations (i.e. the nodal displacements and the nodal velocities) to the gradients of the corresponding cell stresses. The cell stresses, on the other hand, are decomposed into hydrostatic and deviatoric components. The hydrostatic stress is related to the cell density and internal energy by the equation of state, whereas the deviatoric stress is related to

the deviatoric strains, deviatoric strain rates, and temperature via the strength model. As will be discussed in more detail in section 2.3, the equation of state and the strength model are material specific relations defined by the materials constitutive model. The material density is defined by the mass conservation equation, whereas the internal energy density is defined by the energy conservation equation. The temperature is related to the internal energy density using an adiabatic condition and the material specific heat. Deviatoric strains and deviatoric strain rates are computed respectively using the corresponding nodal displacements and nodal velocities. Thus the conservation equations and the materials models define a set of self-consistent equations whose solution yields the temporal and spatial evolutions of the dependent variables listed above.

In the present work, both the Lagrange and Euler processors are used. The Lagrange processor was used to model the sand and all the structural components of the VIMF. The gaseous mine-detonation products and the air surrounding the VIMF are modelled using the higher-order single-material Euler-FCT processor where FCT stands for flux corrected transport. Different regions of the mine/air/VIMF/sand model are allowed to interact and self-interact using the AUTODYN interaction options as described below.

The key feature that makes AUTODYN extremely powerful for solving coupled problems such as impact, explosion, *fluid-structure* interactions, etc., is its ability to model interactions between different regions of the physical model as well as self-interactions of the regions. The way the regions interact depends on the type of processor used to represent the phenomena being modelled. In general, the interactions are classified as joint interactions and impact/slide interactions.

When two domains are joined, their corresponding nodes are fused together and will remain joined throughout the calculation. In other words, joined regions act as single regions.

When two Lagrange domains undergo an impact/slide interaction, the nodes on the surface of one domain are constrained to interact with the nodes on the surface of the other domain. The impact/slide interactions allow the inclusion of friction as well as of gaps which may open and close during the calculation. Self impact/slide interactions may also be defined within a single region. The interaction algorithm is based upon the use of a small detection gap, which defines an interaction detection zone around each interacting face. Whenever a node enters this detection zone, it is repelled using a momentum conserving interaction law, which prohibits penetration of the two interacting surfaces.

When an Euler region interacts with a Lagrange region, the boundary conditions on both regions are changed along the Euler/Lagrange interface. That is, on an Euler/Lagrange interface, the Lagrange region acts as a geometric boundary to the adjoining Euler region, whereas the Euler region provides a pressure boundary to the Lagrange region. As the Lagrange region moves and distorts during calculation, it fills and empties the fixed Euler cells. To avoid the formation of extremely small Euler cells that could greatly reduce the computational time-step, such cells are automatically merged with larger neighbours.

To overcome the problems associated with the mesh distortions caused by large motions of a Lagrange grid, an erosion algorithm is implemented in AUTODYN [**9**], which allows a cell to be removed from the calculation if a pre-defined instantaneous or incremental geometric strain, or effective plastic strain, is exceeded. When a cell is eroded, the mass of the cell can either be discarded or retained at the corner nodes of the cell. If the mass is retained, conservation of inertia and its spatial continuity are maintained during the erosion process. If the retained-inertia option is used and the cells surrounding a particular node are eroded, the node becomes a free node. Free nodes are allowed to continue to interact with impact/slide boundaries and load other bodies. When a node is eroded, the compressive strength of the material within the associated cells is lost and the mass discarded (unless the retained-inertia option is used). For this reason, large erosion strains (typically 1.5–2) are chosen so that cells are not eroded until they are quite severely deformed and their compressive strength and/or mass are not likely to affect the results. Previous work has demonstrated that when the retained inertia option is used excellent results are obtained for the tracking of the motions of the eroded Lagrange cells [**9**].

2.3 Materials constitutive models

As discussed in the previous section, the complete definition of a transient non-linear dynamics problem entails the knowledge of the materials models that define the relationships between the flow variables (pressure, mass density, energy density, temperature, etc.). These relations typically involve an equation of state, a strength equation, and a failure equation for each constituent material. These equations arise from the fact that, in general, the total stress tensor can be decomposed into a sum of a hydrostatic stress (pressure) tensor (which causes a change in the volume/density of the material) and a deviatoric stress tensor (which is responsible for the shape change of the material). An equation of state then is used to define the

corresponding functional relationship between pressure, density, and internal energy (temperature), whereas a strength relation is used to define the appropriate equivalent plastic strain, equivalent plastic strain rate, and temperature dependences of the equivalent deviatoric stress. In addition, a materials model generally includes a failure criterion, i.e. an equation describing the (hydrostatic or deviatoric) stress and/or strain condition(s) that, when attained, causes the material to fracture and lose its ability to support normal and shear stresses.

In the present work, the following three materials are utilized within the computational domain: air, AISI 4340 steel, and sand. In the following sections, a brief description is given of the models used for each of the three constituent materials. The values of all the material parameters defined in the remainder of the section are available in the AUTODYN materials library [**9**]. The data cannot be disclosed here due to copyright violation concerns.

2.3.1 Air

Air is modelled as an ideal gas and, consequently, its equation of state is defined by the ideal-gas gamma-law relation as [**9**]

$$P = (\gamma - 1)\frac{\rho}{\rho_0}E \tag{1}$$

where P is the pressure, γ the constant-pressure to constant-volume specific heats ratio (1.4 for a diatomic gas like air), ρ_0 (1.225 kg/m^3) is the initial air mass density, and ρ is the current density. For equation (1) to yield the standard atmosphere pressure of 101.3 kPa, the initial internal energy density E is set to 253.4 kJ/m^3, which corresponds to the air mass specific heat of 717.6 J/kg K and a reference temperature of 288.2 K.

Owing to the use of a single-material Euler-FCT processor for the gas-phase region, the landmine detonation products are not modelled as a separate material within the gas phase. Rather, the landmine detonation products are modelled initially as a cylindrically shaped air region with a high density ρ and a high internal energy density. Following Fairlie and Bergeron [**14**], the initial density of the detonation products is taken to be the density of the solid TNT explosive and the initial internal energy of this gas is determined by converting the value of the Chapman–Jouget internal energy per unit volume to the corresponding value of the internal energy per unit mass. The corresponding detonation products pressure and the fireball temperature are computed using standard thermodynamic relations.

Since air is a gaseous material and has no ability to support either shear stresses or negative pressures, no strength or failure relations are required for this material.

2.3.2 AISI 4340 steel

In the present work, all the structural components of the VIMF including the witness plate are assumed to be made of the AISI 4340 steel plates. For inert solid materials like AISI 4340 steel, a linear type of equation of state is typically used, which assumes a Hooke's law type relationship between the pressure and the volume change as

$$P = K\mu \tag{2}$$

where K is the bulk modulus of the material and $\mu = (\rho/\rho_0 - 1)$ is the compression ratio. Within the AUTODYN material database, the initial material density ρ_0, the bulk modulus K, the specific heat, and the reference temperature are defined for AISI 4340 steel.

To represent the constitutive response of AISI 4340 steel under deviatoric stress, the Johnson–Cook model is used. This model is capable of representing the material behaviour displayed under large-strain, high deformation rate, high-temperature conditions, of the type encountered in problems dealing with the interactions of detonation products and solid structures. Within the Johnson–Cook model, the yield stress is defined as

$$Y = \lfloor A + B\varepsilon_{\mathrm{pl}}^{\mathrm{n}} \rfloor [1 + C_1 \ \log \ \dot{\varepsilon}_{\mathrm{pl}}][1 - T_{\mathrm{H}}^{\mathrm{m}}] \tag{3}$$

where $\varepsilon_{\mathrm{pl}}$ is the equivalent plastic strain, $\dot{\varepsilon}_{\mathrm{pl}}$ is the equivalent plastic strain rate, A is the zero plastic strain, unit plastic strain rate, room temperature yield stress, B is the strain hardening constant, n is the strain hardening exponent, C_1 is the strain rate constant, m is the thermal softening exponent and $T_{\mathrm{H}} = (T - T_{\mathrm{room}})/(T_{\mathrm{melt}} - \mathrm{T}_{\mathrm{room}})$ is a room temperature (T_{room}) based homologous temperature, while T_{melt} is the melting temperature. All temperatures are given in Kelvin. It should be noted that no plastic deformation of the VIMF or the witness plate is generally observed both in the experiments [**11**] and in the present computer modelling study. Nevertheless, the strength model for AISI 4340 steel was used to be able to detect the potential onset of plasticity.

Since no damage/failure of the VIMF or the witness plate occurs during its use, no failure model is used for AISI 4340 steel.

2.3.3 Sand

Sand has generally a complex structure consisting of mineral solid particles, which form a skeleton. The pores between the solid particles are filled with

effectively dry air (this type of sand is generally referred to as dry sand), with water (saturated sand) or with a two-phase water/air mixture (unsaturated sand). The relative volume fractions of the three constituent materials in the sand (the solid mineral particles, water, and air) are generally quantified by the porosity, α, and the degree of (water) saturation (saturation ratio), SR, which are respectively defined as

$$\alpha = \frac{V_{\mathrm{p}}}{V} \tag{4}$$

and

$$\mathrm{SR} = \frac{V_{\mathrm{w}}}{V_{\mathrm{p}}} \tag{5}$$

where V_{p} is the volume of void (pores), V_{w} is the volume of water, and V is the total volume.

Surface roughness and the presence of inorganic/organic binders are generally considered to be the main causes for friction/adhesion at the inter-particle contacting surfaces. Deformation of the sand is generally believed to involve two main basic mechanisms [**14**–**17**]: (a) elastic deformations (at low pressure levels) and fracture (at high pressure levels) of the inter-particle bonds; and (b) elastic and plastic deformations of the three constituent materials in the sand. The relative contributions of these two deformation mechanisms as well as their behaviour are affected primarily by the degree of saturation of sand and the deformation rate. Specifically, in dry sand the first mechanism controls the sand deformation at low pressures, whereas the second mechanism is dominant at high pressures and the effect of deformation rate is of a second order. In sharp contrast, in saturated sand very low inter-particle friction diminishes the role of the first deformation mechanism. On the other hand, the rate of deformation plays an important role. At low deformation rates, the water/air residing in the sand pores is squeezed out during deformation and, consequently, the deformation of the sand is controlled by the deformation of the solid mineral particles. At high pressures, on the other hand, water/air is trapped within the sand pores and the deformation of the sand is controlled by the deformation and the volume fractions of each of the three constituent phases.

Within AUTODYN, the dynamic response of sand is represented using a compaction materials model that was formulated using the experimental results obtained by Laine and Sandvik [**18**]. A brief description of the original compaction materials model for sand as well as its modification, as proposed in the present authors' recent work [**1**], are discussed below.

2.3.3.1 Compaction equation of state

The original 'compaction' equation of state for sand is based on a piece-wise linear pressure-density relation schematically shown in Fig. 2. It should be noted that, since pressure does not depend explicitly on the internal energy, this relation is equivalent to the standard Mie–Gruneisen equation of state in which the Gruneisen gamma parameter, $\Gamma = v(\partial P/\partial E)_v$, is set to zero. This means that the model would give a more reliable material response under the conditions when either the energy absorbed is not very high (e.g. when the applied pressure levels are not significantly larger than the pressure levels at which the porous material crushes and compacts into a solid material), when the initial material porosity is small or when the magnitude of the Gruneisen gamma parameter is near zero.

Within the AUTODYN computer program [**9**], the initial density of the porous material at a zero pressure level, P_1, is denoted as ρ_1. As the pressure is applied, the relation between the pressure and the density (denoted in Fig. 2 as 'plastic compaction') is defined using up to ten (ρ,P) pairs of values. This portion of the pressure versus density relation is associated with a permanent, plastic compaction of sand. Full compaction of the sand corresponds to the last pair of the (ρ,P) values of the plastic compaction curve.

An increase in pressure beyond the point of full compaction is defined by the following elastic loading linear pressure–density relation:

$$P = C_{\mathrm{s}}^2(\rho - \rho_{\mathrm{s}}) \tag{6}$$

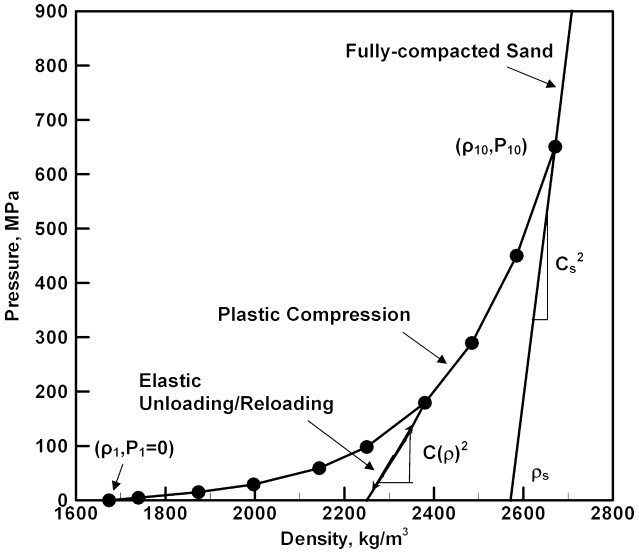

Fig. 2 Pressure versus density relations for dry sand as defined in the AUTODYN materials library [**9**]

where C_s is the sound speed in fully compacted sand at zero pressure and ρ_s is the mass density of the fully compacted sand under a zero applied pressure.

Elastic unloading/reloading of a porous material like sand at any level of compaction is generally governed by the following differential equation

$$\frac{\partial P}{\partial \rho} = C^2(\rho) \tag{7}$$

where C is the sound speed in sand at a density ρ. As indicated in Fig. 2 by the curves denoted as elastic unloading/reloading, the pressure–density relation during elastic unloading/reloading is not linear, which is due to the fact that the sound speed in sand is a function of the material density. Within AUTODYN [**9**], density dependence of the sound speed, C, is defined as a piece-wise linear relation in terms of up to ten (ρ,C) pairs of values.

The original compaction equation of state described above does not include two very important factors controlling the dynamic response of sand under the blast loading conditions, i.e. the effects of the degree of saturation and the deformation rate. In the present authors' previous work [**1**], the original compaction equation of state for sand was modified in order to incorporate these two effects. The modifications of the compaction equation of state for sand were based on the following set of assumptions.

1. The average sand particle size, particle size distribution, and the presence of inorganic/organic natural matter in sand have a second-order effect on the dynamic constituent response of the sand. This assumption was justified by the experimental observations reported in reference [**2**], which clearly showed that the effect of sand type (e.g. prairie sand containing high level of silt and clay, impurity-free −30/+50 sand, etc.), on the detonation-induced momentum transfer to the instrumented horizontal mine-impulse pendulum was small in comparison with the effect of the degree of saturation.
2. The dynamic mechanical response of the sand at any degree of saturation can be obtained as a linear combination of the corresponding dynamic material behaviours for the dry and the saturated sand.
3. The dynamic mechanical response of the dry sand is not rate dependent and it can be represented by the original compaction model implemented in AUTODYN [**9**].
4. The initial density of the saturated sand, $\rho_{1,\mathrm{sat}}$, can be calculated using densities of the solid material in the sand, ρ_s, and water, ρ_w, and the known level of sand porosity, $\alpha = 1 - (\rho_1/\rho_s)$, as

$$\rho_{1,sat} = \rho_s(1-\alpha) + \rho_w\alpha \tag{8}$$

5. When the saturated sand is subjected to relatively low deformation (compression) rates, water is given enough time to leave the pores, and hence the density of the fully compacted sand and the pressure at which full compaction is attained are identical to their counterparts in the dry sand.
6. When the saturated sand is subjected to very high compression rates, water will be trapped inside the pores and, due to a very low compressibility of the water, the compressibility of the sand is controlled by the compressibility of its solid phase. In other words, the saturated sand behaves as a fully compacted sand under high deformation rates and can only undergo an elastic compaction. It should be noted that, while it is a common approach to treat water trapped inside the sand under high strain-rate conditions as an incompressible fluid, in the present work water is considered as a compressible fluid with a bulk modulus of 2.15 GPa. The curve labelled 'high deformation rate' for the saturated sand differs from the one labelled 'fully compacted sand' for dry sand, in Fig. 3, in two respects: (a) the density of saturated sand is lower in this case since the density of water is lower than the density of sand solid particles; and (b) the slope of the first curve is lower since the bulk modulus of water is lower than that of the solid sand particles.

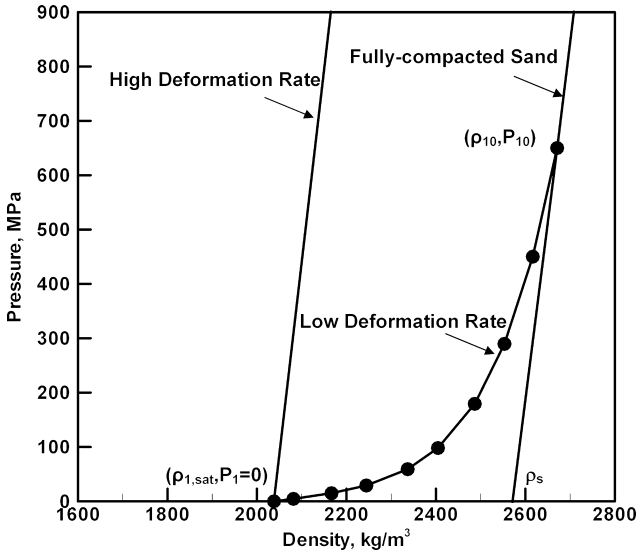

Fig. 3 Pressure versus density relations for saturated sand at low and high deformation rates proposed in reference [**1**]

7. Under intermediate deformation rates, the dynamic material response of the saturated sand can be obtained using a linear interpolation of the high- and low-deformation rate behaviours of the saturated sand. A value of $1.0 \cdot 10^5\,\mathrm{s}^{-1}$ is used as the '*high*' deformation rate, $\dot{\varepsilon}_{\mathrm{high}}$, and a value of $1.0 \cdot 10^{-3}\,\mathrm{s}^{-1}$ is used as the 'low' deformation rate, $\dot{\varepsilon}_{\mathrm{low}}$. At the deformation rates exceeding $1.0 \cdot 10^5\,\mathrm{s}^{-1}$ and at the deformation rates below $1.0 \cdot 10^{-3}\,\mathrm{s}^{-1}$, the dynamic behaviour of sand is assumed to be rate independent and to correspond to the dynamic sand behavior at the respective ($1.0 \cdot 10^5$ or $1.0 \cdot 10^{-3}\,\mathrm{s}^{-1}$) deformation rates. The linear interpolation of the dynamic sand behaviour at the intermediate deformation rates was based on the logarithms of the deformation rates as

$$\rho = \rho_{\mathrm{high}} + (\rho_{\mathrm{low}} - \rho_{\mathrm{high}})\left(\frac{\log\ \dot{\varepsilon} - \log\ \dot{\varepsilon}_{\mathrm{high}}}{\log\ \dot{\varepsilon}_{\mathrm{low}} - \log\ \dot{\varepsilon}_{\mathrm{high}}}\right) \tag{9}$$

where the densities ρ, ρ_{high}, and ρ_{low} correspond respectively to the deformation rates $\dot{\varepsilon}$, $\dot{\varepsilon}_{\mathrm{high}}$ and $\dot{\varepsilon}_{\mathrm{low}}$ and are all associated with the same level of pressure. The computational results obtained are found not to be significantly affected by an order of magnitude changes in the values for the high- and low-deformation rates.
8. Since the irreversible plastic deformation of sand is dominated by the plastic deformation behaviour of its solid phase, it is assumed to be independent of the degree of saturation and the rate of deformation. In other words, only the equation of state in the original compaction model was modified in reference [**1**] following the aforementioned procedure. Following the preliminary study reported in the present authors' previous work reference [**8**], the strength compaction model has been modified in the present authors' recent work [**27**] to account for the inter-particle water-induced lubrication effect, which lowers the sand's yield strength. Details of this modification are presented below.

The pressure versus density relationships corresponding to the original compaction model for sand and also for dry sand at a porosity level of 38 percent are displayed in Fig. 2. The pressure versus density relationships corresponding to saturated sand in the present formulation with a porosity level of 38 percent are displayed in Fig. 3. It should be noted that the pressure versus density curve labelled 'high deformation rate' in Fig. 3, which was originally reported in reference [**1**] has been corrected to account for the fact that the compressibility of the solid mineral particles in the saturated sand rather than the overall compressibility of the saturated sand is equal to that in the fully compacted dry sand. The new equation of state is implemented in the user subroutine 'mdeosuser.f90' and interfaced with the AUTODYN computer program [**9**].

2.3.3.2 Compaction strength model

The 'compaction' strength model for sand is based on an isotropic, perfectly plastic, rate independent yield-surface approximation and postulates that the yield stress depends explicitly on pressure and not on material density. Within the AUTODYN program [**9**], the relationship between the yield stress, Y, and pressure, P, is defined as a piece-wise linear function consisting of up to ten (P,Y) pairs of values. The yield stress quantifies the resistance of the material to a plastic (irreversible) shape change. The plastic shape change occurs when the magnitude of the second invariant of the deviatoric part of the stress tensor becomes equal to the yield stress.

Unloading (and subsequent reloading) of a previously plastically deformed material is of an elastic (reversible) nature and, in this case, the deviatoric stress is proportional to the deviatoric strain with the proportionality constant being equal to the shear modulus, G. In a porous material such as sand, the shear modulus is a function of the material density. The 'compaction' G versus ρ relation is defined within AUTODYN [**9**] as a piece-wise linear function using up to ten (ρ,G) pairs of data.

The original strength compaction model has been modified in the present authors' recent work [**19**] to account for the fact that water acts as an inter-particle lubricant and reduces the shear strength of the sand. The modification of the original strength compaction model was carried out as follows.

1. It is first recognized that the ratio of the shear strength to the pressure for the entire range of pressures in the original yield strength versus pressure relation for dry sand yields an effective friction coefficient in a narrow range between 1.25 and 1.35.
2. The presence of water in the fully saturated sand creates a water-based shear layer physically separating sand particles and reduces the effective friction coefficient and, thus the shear strength.
3. While the thickness of such a layer (and thus the magnitude of the inter-particle friction coefficient) is dependent on the rate of deformation, only pressure-dependent values of the inter-particle friction coefficient in the limit of infinite deformation rates of the saturated sand are used.
4. Following the work of Dowson and Ehret [**20**], the values of the inter-particle friction coefficient in the saturated sand are set to vary between 0.1 at

the lowest pressures and 0.8 at the highest pressure. The yield strength at a given pressure level is then defined as a product of the friction coefficient and the pressure.

5. A detailed account of the revisions made in the original compaction model for sand has been reported in the present authors' recent correspondence [**19**].

2.3.3.3 Failure model

The failure behaviour of sand is modelled within the AUTODYN materials database by specifying a minimum (negative) value of the hydrodynamic pressure below which the material fractures lose its ability to support any tensile or shear stress. However, if a given 'fractured' material region is subsequently subjected to positive pressures, it is given an ability to reheal and close up its cracks. A zero value of the hydrodynamic pressure was used in the present work. The results reported in section 3 were found to be fairly insensitive to the choice of the minimum pressure over a relatively large range of negative pressures.

2.4 Problem definition and computational analysis

In this section, a brief description is given of the computational analysis used to simulate the interaction of the detonation-products/soil ejecta resulting from the explosion of a shallow buried mine and the VIMF. The computational modelling of this interaction involved two distinct steps: (a) geometrical modelling of the VIMF along with the adjoining mine, air, and sand regions; and (b) the associated transient non-linear dynamics analysis of the impulse loading (momentum transfer) from the detonation-products/soil ejecta to the VIMF structure. The part (b) of this analysis was performed using the technique developed by Fairlie and Bergeron [**14**]. This technique couples an Eulerian-FCT mesh, which models the rapidly expanding blast gases and the (initially stationary) air, to a Lagrangian mesh, which is used to model the soil, witness plate, and VIMF. The soil and VIMF are modelled using eight node solid elements, whereas the witness plate is modelled using shell elements.

An advantage was taken of the inherit symmetry of the model. In other words, two mutually-orthogonal vertical planes of symmetry were placed along the axis of the VIMF as well as along the axis of the air, mine, and sand regions, which enabled only a quarter of the computational model to be analysed. Representative quarter symmetric models for various computational domains used in the present study are shown in Fig. 4. It should be noted that the

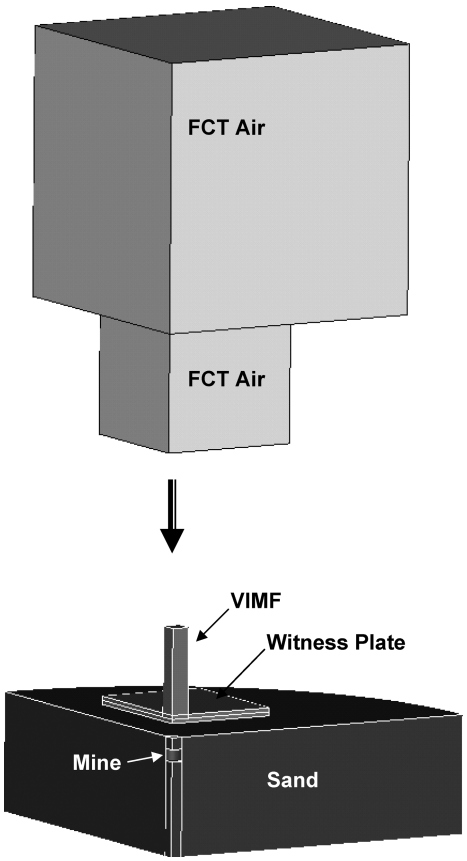

Fig. 4 Computational sub-domains used in the present work

lower Eulerian-FCT domain is located within the soil, whereas the upper one extends above the soil.

The lower Eulerian-FCT domain located within the soil contains a region of pressurized air to represent the blast gas products (denoted as mine in Fig. 4). The remainder of the lower Eulerian-FCT domain and the upper Eulerian-FCT domain were assigned standard (ambient) air properties. The material model used for air was reviewed in section 2.3.1.

Both the witness plate and the VIMF mass were modelled as AISI 4340 steel whose constitutive relations were reviewed in section 2.3.2. Welded joints of the different structural components of the VIMF were simulated by joining the components in question.

Sand was modelled using Lagrangian elements that were set to erode at an incremental geometric strain of 2.0. The mass of the nodes was retained and in analysis involving structural interaction, the eroded nodes interact with the structure. The material model used for sand was reviewed in section 2.3.3.

The air/sand and air/VIMF interactions are accounted for using the appropriate Euler/Lagrange coupling option within AUTODYN [**9**]. Likewise, the sand/VIMF interactions were modelled through

the use of the appropriate Lagrange/Lagrange coupling option.

The 'flow out' boundary conditions were applied to all the free faces (the faces which do not represent interfaces between the different domains) of the Euler-FCT domain except for the face associated with the vertical symmetry planes. To reduce the effect of reflection of the shock waves at the outer surfaces of the Lagrange sand domain, 'transmit' boundary conditions were applied to all the free faces of this domain except for the face associated with the vertical symmetry planes and the upper face that defines the sand/air and sand/VIMF interfaces. The transmit boundary conditions enable the propagation of pressure waves across the boundaries without reflection mimicking wave propagation in an infinitely large sand domain [**9**].

Several gauge points were defined within the landmine, sand, air, witness plate, and the VIMF, which allowed monitoring of the quantities such as pressure, velocity, and (in the case of the Lagrange domains) of the vertical displacements.

At the beginning of the simulation, all the Lagrange and Euler-FCT domains are activated and the landmine detonated. As explained earlier, the detonated landmine was initially modelled as a circular disc-shaped high mass-density, high energy-density sub-domain within the lower Euler-FCT region.

It should be noted that the following assumptions/simplifications were used in the present analysis when accounting for the heat effect accompanying the detonation of a mine and the subsequent interactions between the detonation products and sand ejecta with the VIMF structure: (a) an adiabatic condition is assumed, thus no heat conduction is considered; (b) PV-work, associated with the plastic-compaction of the sand as well as the work associated with inter-particle friction are dissipated in the form of heat and the resultant increase is assessed using the materials effective specific heat; and (c) no thermal effect associated with the viscous flow of water or from water boiling/evaporation are considered.

A standard mesh sensitivity analysis is carried out in order to ensure that the results obtained are insensitive to the size of the cells used.

3 RESULTS AND DISCUSSION

3.1 Modified compaction model validation in the case of fully saturated sand

The transient non-linear dynamics analysis described in section 2.4 is carried out in the present section in conjunction with the modified compaction materials model for sand described in section 2.3.3 to examine the potential of such an analysis to quantify the blast loads associated with detonation of landmines buried in fully saturated sand. This was done by comparing the model predictions regarding the total impulse captured by the witness plate with their experimental counterparts obtained in the work of Taylor *et al.* [**11**], who carried out large-scale experiments using the VIMF at the Army Research Laboratory, Aberdeen, MD. The test conditions used in the work of Taylor *et al.* [**11**] are summarized in Table 1. It should be noted that two different witness plates were used with the respective length by width by thickness dimensions of 2.43 m by 2.82 m by 0.088 m and 1.83 m by 3.65 m by 0.088 m.

A comparison between the experimental results and their computational counterparts is given in Table 2. To demonstrate the quantitative improvements brought about by the modified compaction model for sand, the corresponding computational results obtained using the original compaction model are also shown in Table 2. An examination of the results shown in this table reveals that for each of the test conditions studied by Taylor *et al.* [**11**], the use of the modified compaction model for sand yields an improved agreement with the experimental findings. In some cases, e.g. test numbers 5 and 8 the agreement between the model

Table 1 VIMF set-up and test conditions [**11**]

Test no.	Charge mass (kg)	Charge diameter, (m)	Charge height (m)	DoB[a] (m)	HoT[b] (m)	VIMF target total mass (kg)
1[c]	4.54	0.254	0.56	0.10	0.40	12 506
3[c]	4.54	0.254	0.56	0.30	0.40	12 506
4[c]	4.54	0.254	0.56	0.10	0.20	12 506
4a[d]	4.54	0.254	0.56	0.10	0.20	11 852
5[d]	2.27	0.152	0.76	0.80	0	11 852
6[d]	4.54	0.254	0.56	0.10	0.40	11 852
7[d]	2.27	0.152	0.76	0.81	0.16	11 535
8[d]	7.47	0.236	0.86	0.10	0.40	11 535

[a]DoB = Depth of burial.
[b]HoT = Height of the target plate above the soil.
[c]Witness plate size: 2.43 m by 2.82 m by 0.088 m.
[d]Witness plate size: 1.83 m by 3.65 m by 0.088 m.

Table 2 Measured and computed impulse transferred to the VIMF witness plate

Test no.	Measured total impulse (Ns)	Computed total impulse modified sand model (Ns)	computed total impulse original sand model (Ns)
1	71 801	86 879	19 353
3	74 017	67 355	18 786
4	81 125	94 916	21 519
4a	69 644	61 287	17 903
5	77 612	80 716	20 211
6	59 286	76 479	15 241
7	36 938	42 109	9619
8	94 390	91 558	23 776

predictions and their experimental counterparts is exceptionally good. As discussed in the present authors' previous work [**1**], the main two reasons for the original compaction model for sand underpredicting the magnitude of the transferred impulse at high levels of the moisture content are: (a) too high compressibility of the sand, which promotes explosion-energy dissipation through irreversible compaction of the sand; and (b) a lack of consideration of the reduction of the sand's yield stress due to moisture-induced inter-particle lubrication effects, which limits the extent of sand ejection.

It should be recalled that the behaviour of detonation products and air was represented using an ideal gas model, which may not be fully justified due to high-pressure/high-temperature conditions encountered in the vicinity of an exploded charge. To assess the effect of this choice of the materials model for air, few calculations were repeated using the real-gas Nobel–Able equation of state [**21**] instead of the ideal-gas equation. The results obtained (not shown here for brevity) revealed that the choice of the materials model for air had a minor effect of the momentum transfer results. It should be also noted that the work of Raftenberg [**22**] clearly established that a combination of the linear equation of state and the Johnson–Cook strength and failure models like the one used in the present work can quite realistically represent the response of the AISI 4340 steel under ballistic loading conditions. With the improvements in the materials model for sand reported in this section and in the present authors' previous work [**1**] relative to the original compaction model for sand [**18**], it appears that materials models for air, structural metallic materials like the AISI 4340 steel and sand are all at comparable levels of their ability to account for the behaviour of these materials under impulse loading conditions accompanying detonation of shallow buried and ground-laid mines.

An example of the pressure field in air during detonation of a land mine buried in the saturated sand is shown in Fig. 5. For clarity, the sand and the VIMF regions of the computational domain are denoted in Fig. 5 using a uniform material-specific colour.

3.2 Shock-type versus bubble-type impulse loading

In addition to measuring the total blast impulse transferred to the VIMF, Taylor *et al.* [**11**] also recorded the position of the witness plate continuously from the time of detonation until the time it returned to its initial position. This allowed them to determine the temporal evolution of the plate velocity and to get a good estimate of the (maximum) initial plate velocity, V_0. Since the witness plate did not suffer any visible permanent deformation or damage, the blast impulse results shown in Table 2 were then obtained as a product of this velocity and the VIMF witness plate mass. It should be noted that this approach is justified because the time during which the explosion products and the soil ejecta interact with the witness plate (typically 0.2–0.3 ms) is small compared to the response time of the plate (generally 12–15 ms for an approximately 12 ton plate).

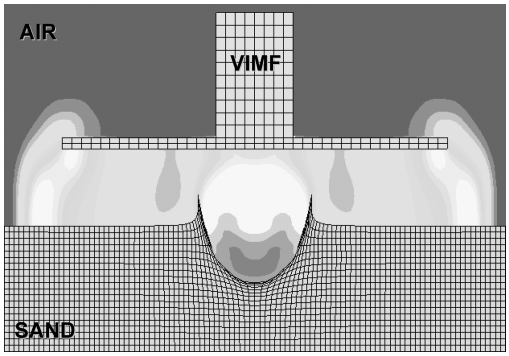

Fig. 5 An example of the pressure field in air during detonation of a mine shallow buried in saturated sand

A typical result obtained by Taylor *et al.* [**11**] pertaining to the position of the target plate as a function of time is shown in Fig. 6. The results shown in Fig. 6 indicate that the witness plate briefly stops moving upward in a time period between 17 and 25 ms and then re-accelerates. This finding was explained by Taylor *et al.* [**11**] as follows: when the depth of burial of a charge in the saturated sand is

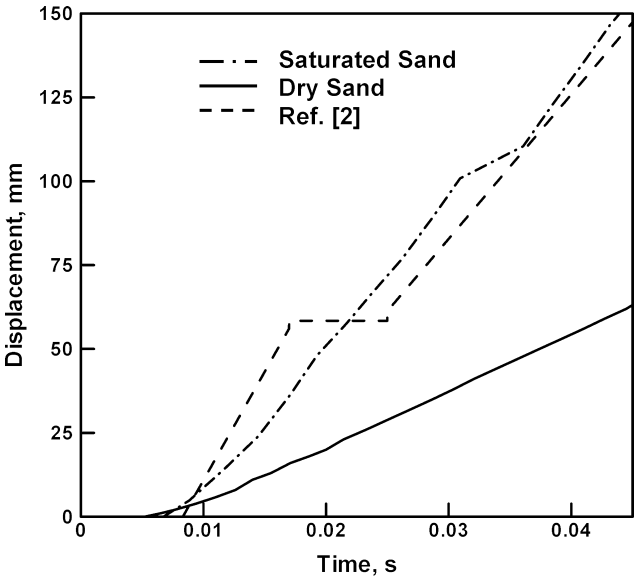

Fig. 6 Temporal evolution of the witness plate's displacement for Test 4 as specified in Table 1

large enough (typically at least 10 cm) to enable significant attenuation of the wave strength and prevent a burst of the sand overburden, a large acoustic impedance mismatch between saturated sand and air causes the shock wave travelling through the soil to be almost entirely reflected back, as a rarefaction wave, into the sand at the soil/air interface. Consequently, a target located in the air above the landmine experiences very little shock loading from the explosion. Under these conditions, the explosion induced loading of the target structure (while still of an impulsive nature) is, using the UNDEX (under water explosion) terminology, of a bubble type rather than of a shock type [**22**–**26**]. In other words, saturated sand tends to behave, in some respect, more like a fluid than a solid material. A bubble containing the high-pressure detonation products, which is formed within the saturated sand undergoes an initial rapid expansion and the inertia of the outward moving sand carries it far beyond the point of pressure equilibrium. The expansion stops only after the gas pressure has fallen substantially below the ambient pressure. Then, the higher surrounding pressure reverses the motion and the bubble begins to shrink causing its inner pressure to increase. The reverse motion also overshoots the equilibrium and when the bubble reaches its minimum size, the gas is re-compressed to a high pressure. At this point, a second 'explosion' effectively takes place and the whole bubble oscillation process repeats. When the over-expanded bubble is temporarily trapped between the soil and the target, it can pull down on the target and reduce its vertical velocity, as observed in Fig. 6. These complex interactions between the explosion bubble and the target are the reason why Taylor *et al.* [**11**] utilized the short-time data shown in Fig. 6 to estimate V_0 rather then employing the more common method based on the use of the maximum height to which the target plate rises.

To examine whether the extent of water saturation of the sand has indeed an effect on the nature of the blast (shock versus bubble) loading, as postulated by Taylor *et al.* [**11**], the impulse transferred to the witness plate by the air alone is monitored both in the case of dry sand and in the case of saturated sand. The results obtained show that despite the fact that the total impulse transferred to the plate is larger by 260 to 300 per cent in the case of saturated sand, Table 2, the impulse transferred by the air alone is 5–10 per cent smaller in the case of saturated sand. Likewise, the pressure versus time traces at a gauge point located in air along the vertical axis of the computational domain at a distance of 2 cm below the witness plate, Fig. 7, clearly shows that the intensity of the blast wave is lowered in the case of saturated sand. The results displayed

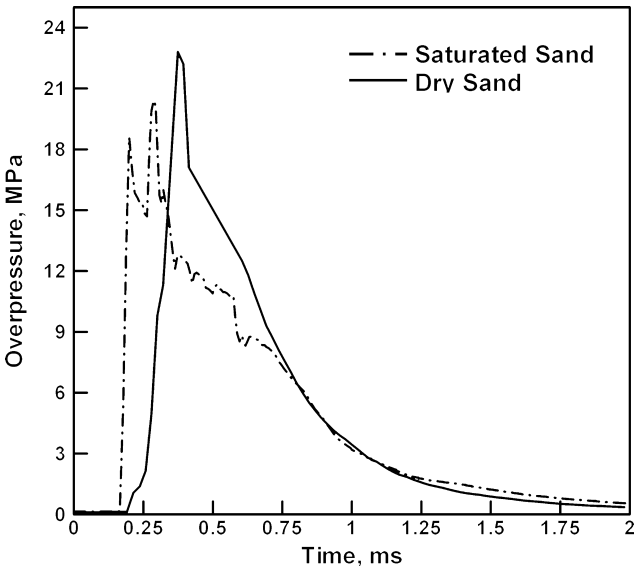

Fig. 7 Temporal evolution of the overpressure in air at a point located along the vertical axis 2 cm below the witness plate for Test 4 as specified in Table 1

in Fig. 7 can be explained as follows: there is a substantially larger difference in the acoustic impedances of saturated sand and air, on one hand, and of dry sand and air, on the other. The acoustic impedance of a material is defined as a square root of the product of the material's mass density and its bulk modulus. The initial acoustic impedance of saturated sand is approximately 3370 times larger than that of air, whereas the initial acoustic impedance of dry sand is only 484 times larger than that of air. Consequently, the compression blast wave resulting from detonation of the landmine and travelling through sand will reflect more at the sand/air interface in the case of saturated sand and be transmitted more in the case of dry sand. According to the basic theory of acoustics, the acoustic impedance mismatch at the saturated-sand/air interface and the dry-sand/air interface result in the reflected energy fraction of approximately 0.9994 and 0.9958, respectively. The reflected energy fraction at an interface is defined as a square of the ratio of the difference and the sum of the acoustic impedances of the two adjoining materials. It should be noted, that in the case of shock waves, one should use the shock impedance (dependent on a shock velocity) rather than the acoustic impedance (dependent on a sound velocity) to determine the ratio between the transmitted and reflected pressure/energy. Thus, the aforementioned analysis based on the acoustic impedance should be considered only as a rough approximation to the one based on the shock-impedance ratio.

To further examine the effect of the saturation content of the sand on the nature of the blast loading, pressure was monitored as a function of time at several points in sand. An example of the temporal evolution of the pressure at a gauge point located in sand 7.5 cm below the air/sand interface and 5.5 cm away from the vertical axis is displayed in Fig. 8. The results displayed in Fig. 8 clearly show the oscillating nature of the explosion gas bubble in the case of the saturated sand and the absence of such oscillations in the case of dry sand.

Finally, the vertical displacement of the VIMF witness plate as a function of time is monitored for the cases of landmine detonations in the saturated and the dry sand for the test conditions corresponding to those used by Taylor *et al.* [**11**] in conjunction with Fig. 6. The computed results are displayed in Fig. 6 and they suggest that there is a reduction in the upward velocity of the plate in the case of the saturated sand in the time interval close to that in which Taylor *et al.* [**11**] observed a halt in the rise of the plate. No similar velocity reduction is observed in the case of dry sand.

All the findings reported in conjunction with Figs 5–8 indicate that in the case of saturated sand, the oscillation-bubble effects play a more pronounced role in blast loading, whereas the shock waves propagating through the air between the sand/air interface and the air/witness-plate interface make a proportionally lower contribution as suggested by Taylor *et al.* [**11**].

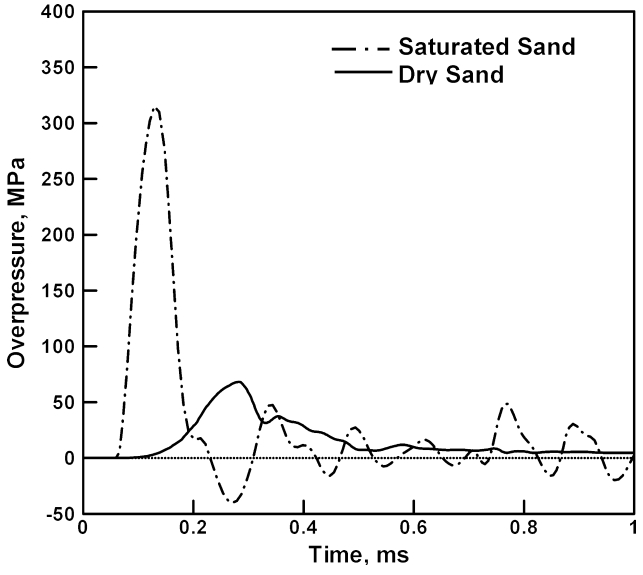

Fig. 8 Temporal evolution of the overpressure in sand at a point located 5.5 cm away from the vertical axis and 7.5 cm below the sand/air interface for Test 4 as specified in Table 1

It should be noted that a possible explanation for the observed differences in the behaviour of the dry and the saturated sand, as suggested correctly by one of the reviewers of the present paper, are previously identified difference in tensile strengths and the character of sand overburden bursting in sand at two extremely different levels of saturation.

4 SUMMARY AND CONCLUSIONS

On the basis of the results obtained in the present work, the following main summary remarks and conclusions can be drawn.

1. The ballistic materials model for sand recently developed by Grujicic *et al.* [**19**], which incorporates the effects of moisture and the rate of deformation substantially improves the agreement between the experimentally measured and computed results pertaining to the landmine detonation phenomena (e.g. momentum transfer, temporal evolution of the target velocity, etc.) with respect to the original compaction model for sand. The main deficiencies of the original compaction model for sand at high levels of the moisture content are too high compressibility of the sand that promotes explosion-energy dissipation through irreversible compaction of the sand and a lack of consideration of the reduction of the sand's yield stress due to moisture-induced inter-particle lubrication effects, which limits the extent of sand ejection.
2. Detonation of the buried landmines in fully saturated sand has some similarities with the under-water explosion, which is associated with the fact that the high strain rate, large-deformation behaviour of the saturated sand resembles more the response of water than does the behaviour of dry sand. Specifically, both the experimental and computational results provide evidence for the formation of an oscillating detonation-products bubble in the saturated sand.

ACKNOWLEDGEMENTS

The material presented in this paper is based on work supported by the US Army/Clemson University Cooperative Agreement W911NF-04-2-0024 and by the US Army Grant Number DAAD19-01-1-0661. The authors are indebted to Drs. Walter Roy and Fred Stanton for the support and a continuing interest in the present work.

REFERENCES

1 **Grujicic, M., Pandurangan, B.,** and **Cheeseman, B.** The effect of degree of saturation of sand on detonation phenomena associated with shallow-buried and ground-laid mines. *J. Shock Vib.*, 2006, **13**, 41–61.

2 **Bergeron, D.** and **Tremblay, J. E.** Canadian research to characterize mine blast output. 16th International MABS Symposium, Oxford, UK, September 2000.

3 **Holsapple, K. A.** and **Housen, K. R.** Crater database and scaling tools, available from http://keith.aa. washinton.edu/craterdata, accessed November 2004.

4 **Westine, P. S., Morris, B. L., Cox, P. A.,** and **Polch, E.** Development of computer program for floor plate response from land mine explosions. Contract report no. 1345, US Army TACOM Research and Development Center, 1985.

5 **Morris, B. L.** Analysis of improved crew survivability in light vehicles subjected to mine blast. Final report for contract no. DAAK70-92-C-0058, US Army Belvoir RDEC, Ft. Belvoir, VA, 1993.

6 **Bergeron, D. Hlady, S.,** and **Braid, M. P.** Pendulum techniques to measure land mine blast loading. 17th International MABS Symposium, Las Vegas, USA, June 2002.

7 **Braid, M. P.** Experimental investigation and analysis of the effects of anti-personnel landmine blasts, Defence R&D Canada, Suffield Special Publication, December 2001, DRES SSSP 2001-188.

8 **Grujicic, M., Pandurangan, B.,** and **Cheeseman, B.** A computational analysis of detonation phenomena associated with mines shallow-buried in sand. *Multidiscipline Model. Mater. Struct.*, accepted for publication, January 2006.

9 **AUTODYN-2D** and **3D**. *User Documentation Version 5.0*, 2004, (Century Dynamics Inc., Concord, CA).

10 **Bergeron, D., Walker, R.,** and **Coffey, C.** Detonation of 100-gram anti-personnel mine surrogate charges in sand-A test case for computer code validation. Suffield report no. 668, Defence Research Establishment Suffield, Ralston, Alberta, Canada, April 1998.

11 **Taylor, L. C., Skaggs, R. R.,** and **Gault, W.** Vertical impulse measurements of mines buried in saturated sand. *Fragblast*, 2005, **9**(1), 19–28.

12 **Gniazdowski, N.** *The vertical impulse measurement facility maintenance and inspection manual*. ARL technical report 2004.

13 **Skaggs, R. R., Watson, J., Adkins, T., Gault, W., Canami, A.,** and **Gupta, A. D.** *Blast loading measurements by the vertical impulse measurement fixture (VIMF)*. ARL technical report, ARL-TR-3383, US Army Research Laboratory, Aberdeen Proving Ground, MD, 2005.

14 **Fairlie, G.,** and **Bergeron, D.** Numerical simulation of mine blast loading on structures. Proceedings of the 17th Military Aspects of Blast Symposium, Nevada, June 2002, pp. 17–22.

15 **Henrych, J.** *The dynamics of explosion and its use*, 1979 chapter 5, (Elsevier Publications, New York, USA).

16 **Loret, B.** and **Khalili, N.** A three-phase model for unsaturated soils. *Int. J. Numer. Analy. Methods Geomech.*, 2000, **24**, 893–927.

17 **Lyakhov, G. M.** *Principles of dynamic explosions in soils and fluid media*, 1964. (Nedra, Moscow).

18 **Laine, P.** and **Sandvik, A.** Derivation of mechanical properties for sand. Proceedings of the 4th Asia-Pacific Conference on *Shock and impact loads on structures*, CI-Premier PTE LTD, Singapore, November 2001, pp. 361–368.

19 **Grujicic, M., Pandurangan, B., Cheeseman, B. A., Roy, W. N.,** and **Skaggs, R. R.** Validation of the modified compaction material model for sand with various degrees of water saturation. *J. Shock Vib.*, submitted for publication, February 2006.

20 **Dowson, D.** and **Ehret, P.** Past, present and future studies in elastohydrodynamics. *Proc. Instn Mech. Engrs, Part J: J. Engineering Tribology*, 1999, **213**, 317–333.

21 **Schwer, D.** and **Kailasanath, K.** *Blast mitigation by water mist (1) simulation of confined blast waves*. Report NRL/MR/6410-02-8636, Naval Research Laboratory, Washington, August 2002.

22 **Raftenberg, M. N.** Close-in blast loading of a steel disc – sensitivity to steel strength modeling. *Int. J. Impact. Eng.*, 1997, **20**, 651.

23 **Van der Veen, W. A.** Crushing simulation of a partially filled fuel tank beyond failure. 2005 SAE World Congress, Detroit, April 2005.

24 **Van der Veen, W. A.** Simulation of a compartmented airbag deployment using an explicit, coupled euler/Lagrange method with adaptive euler domains. NAFEMS 2003, Florida, 2003.

25 **Bloom, F.** Constitutive models for wave propagation in soils. *Appl. Mech. Rev.*, 2006, **59**, 146–175.

26 **Bloom, F.** Wave propagation in partially saturated soils. *Appl. Mech. Rev.*, 2006, **59**, 177–209.

BIBLIOGRAPHY

Wang, Z., Hao, H., and **Lu, Y.** A three-phase soil model for simulating stress wave propagation due to blast Loading. *Int. J. Numer. Analy. Methods Geomech.*, 2004, **28**, 33–56.

APPENDIX

Nomenclature

A	room temperature yield stress
B	strain hardening constant
C	speed of sound
C_1	strain rate constant
E	internal energy
G	shear modulus
K	bulk modulus
P	pressure
SR	saturation ratio
T	temperature
v	specific volume
Y	yield stress

α	porosity
γ	constant-pressure to constant-volume specific heats ratio
Γ	Gruneisen parameter
ε	plastic strain
μ	compression ratio
ρ	density

Subscripts

H	homologous quantity
melt	melting point quantity
p	pore related quantity
pl	plastic state quantity
room	room temperature quantity
s	fully-compacted sand related quantity
sat	saturation related quantity
w	water related quantity

Superscripts

m	thermal softening exponent
n	strain hardening exponent